Photosynth Res (2009) 102:377–390
DOI 10.1007/s11120-009-9490-7

REVIEW

Spin labeling EPR

Johann P. Klare · Heinz-Jürgen Steinhoff

Received: 21 December 2008 / Accepted: 14 August 2009 / Published online: 29 August 2009

Abstract Site-directed spin labeling in combination with electron paramagnetic resonance spectroscopy has emerged as an efficient tool to elucidate the structure and conformational dynamics of biomolecules under native-like conditions. This article summarizes the basics as well as recent progress of site-directed spin labeling. Continuous wave EPR spectra analyses and pulse EPR techniques are reviewed with special emphasis on applications to the sensory rhodopsin–transducer complex mediating the photophobic response of the halophilic archaeum *Natronomonas pharaonis* and the photosynthetic reaction center from *Rhodobacter sphaeroides* R26.

Keywords DEER · Nitroxide · PELDOR · Polarity · Photosynthetic reaction center · Sensory rhodopsin · Spin label accessibility · Spin label mobility

Abbreviations

AS	Amphipathic sequence
CrOx	Chromium oxalate
cw	Continuous wave
DEER	Double electron–electron resonance
EPR	Electron paramagnetic resonance
MTSSL	(1-Oxyl-2,2,5,5-tetramethylpyrroline-3-methyl)methanethiosulfonate spin label
NpSRII	*Natronomonas pharaonis* sensory rhodopsin II
NpHtrII	*Natronomonas pharaonis* halobacterial transducer II
PELDOR	Pulse electron–electron double resonance
PML	Purple membrane lipids
RC	Reaction center
SDSL	Site-directed spin labeling
TM	Transmembrane helix

J. P. Klare · H.-J. Steinhoff (✉)
Physics Department, University of Osnabrück, Barbarastr. 7, 49076 Osnabrück, Germany
e-mail: hsteinho@uni-osnabrueck.de

Introduction

Since the pioneering study of Wayne L. Hubbell and coworkers (Altenbach et al. 1989a; Altenbach et al. 1990) site-directed spin labeling (SDSL) in combination with electron paramagnetic resonance (EPR) spectroscopy has emerged as an efficient tool to elucidate the structure and the conformational dynamics of biomolecules under conditions close to the physiological state of the system under investigation. The technique is applicable to soluble molecules, e.g., proteins and nucleic acids, as well as to membrane proteins either solubilized in detergent or embedded in the lipid bilayer, and the size and complexity of the system under investigation is almost arbitrary (for reviews see, e.g. Bordignon and Steinhoff 2007; Hubbell et al. 1996; Hubbell et al. 1998; Klug and Feix 2008). Spin labels are introduced at selected sites within proteins usually by cysteine substitution mutagenesis followed by modification of the sulfhydryl group with a nitroxide reagent. One of the most commonly used spin label is the methanethiosulfonate spin label (MTSSL) (Fig. 1). Alternatively, nonsense suppressor methodology or solid-phase peptide synthesis can be used to introduce the desired unpaired electron into proteins. In the case of nucleic acids, the spin label can be attached via sulfhydryl-modified nucleobases or sugar moieties introduced at the desired position(s) during solid-phase synthesis of the oligonucleotide. Continuous wave (cw)

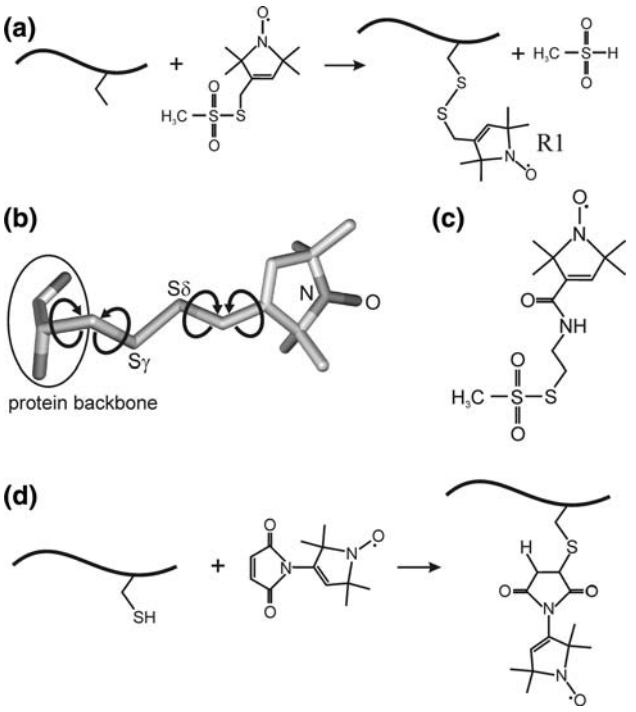

Fig. 1 **a** Reaction of the methanethiosulfonate spin label (MTSSL) with the sulfhydryl group of a cysteine side chain, generating the spin label side chain R1. **b** Flexible bonds within the R1 side chain are indicated. **c** Chemical structure of the MTS-4-oxyl spin label. **d** Reaction of a maleimide spin label *N*-(1-oxyl-2,2,6,6-tetramethyl-4-piperidinyl)maleimide with the sulfhydryl group of a cysteine side chain

EPR spectroscopy of the spin-labeled molecules yields information about the nitroxide side chain mobility, solvent accessibility, the polarity of its immediate environment, and intra- or intermolecular distances between two nitroxides or a single nitroxide and another paramagnetic center in the system. Pulse EPR techniques are emerging, which stretch the range of measurable interspin distances up to 8 nm, thereby matching nicely with the distance range of interest in biomolecules or biomolecular assemblies. The analysis of the EPR data for a series of spin-labeled protein variants allows modeling of the protein structures with a spatial resolution at the level of the backbone fold (Jeschke et al. 2005; Mchaourab and Perozo 2000; Perozo et al. 1998; Vasquez et al. 2008; Wegener et al. 2001). Substrate- or light-induced conformational changes can be followed with sub-millisecond time resolution using time resolved cw detection or characterized by trapping the molecules in activated or intermediate states (Altenbach et al. 2008; Steinhoff et al. 1994).

This article summarizes the basics as well as recent progress in the SDSL methodological approach, with special emphasis on applications to the study of the sensory rhodopsin–transducer complex mediating the photophobic response of the halophilic archaeum *Natronomonas pharaonis* and the photosynthetic reaction center (RC) from *Rhodobacter sphaeroides* R26.

Methods of spin labeling

Spin labeling of cysteines

For the modification of peptides or proteins with spin labels, three different approaches have been established. The most commonly used method utilizes the reactivity of the sulfhydryl group of cysteine residues which are engineered into the protein under investigation applying site-directed mutagenesis. This approach usually requires that the target proteins possess only cysteine residues at the desired sites and that additional cysteines present in the protein can be replaced by serines or alanines. Among the various spin labels available, the (1-oxyl-2,2,5,5-tetramethylpyrroline-3-methyl) methanethiosulfonate spin label (MTSSL) (Berliner et al. 1982) is the most often used in SDSL studies due to its sulfhydryl specificity and its small molecular volume, similar to that of a tryptophane side chain (Fig. 1a). This spin label is bound to the protein by formation of a disulfide bond to the sulfhydryl group of the cysteine, the resulting spin label side chain being commonly abbreviated as R1. The link between the piperidine-oxyl moiety and the protein backbone renders the R1 side chain flexible (see Fig. 1b), thereby minimizing disturbances of the native fold of the protein. The unique dynamic properties of this spin-label side chain provide detailed structural information from the shape of its room temperature EPR spectrum. Nevertheless, the large conformational space accessible for the R1 side chain (the distance between the C_β and the NO group varies between 5 and 8 Å, depending on the conformation) does not allow relating the data obtained directly to the properties of the native side chain replaced by R1. In addition, the flexibility of R1 may result in large distance distributions between two spin labels rather than a sharp defined distance, a drawback which can be encountered by the study of a number of different spin-labeled sites and eventually of conformational searching approaches (see, e.g., Sale and Song 2005). Besides MTSSL, a variety of other different nitroxide radical compounds are commercially available, such as the 1-oxyl-2,2,5,5-tetramethyl, 2,5-dihydro-1H-pyrrol-3-carboxylic acid (2-methanethiosulphonyl-ethyl) amide (MTS-4-oxyl) spin label (Fig. 1c), comprising longer or sterically more demanding linkers. Also, pH-sensitive spin probes have been used to label the thiol group, e.g., of a synthetic peptide fragment of the laminin B1 chain (Smirnov et al.

2004) or of iso-1-cytochrome c from the yeast *Saccharomyces cerevisiae* (Voinov et al. 2008).

Alternatives to the widely used methanethiosulfonate spin labels are maleimide-functionalized spin label compounds (Griffith and McConnell 1966) (Fig. 1d). Their advantage compared to MTS spin labels is the robustness of the linkage toward reducing agents, such as DTT, which leads to immediate release of spin label side chains bound *via* disulfide bonds. However, this method suffers from two major drawbacks. First, the maleimide spin labels are sterically much more demanding compared to the MTSSL and, second, depending on pH, maleimides may also react with primary amines. Whereas at pH 7, the maleimide group is much more reactive toward cysteines than amines, at pH values above 7.5 the reactivity toward primary amines increases. In addition, at pH > 7.5, the maleimide group may undergo hydrolysis, leading to an open unreactive maleamic acid form, before or after sulfhydryl coupling.

Isotope-labeled nitroxide compounds with ^{14}N exchanged by ^{15}N are important for specialized applications. The corresponding EPR spectra are characterized by a two line spectrum (nuclear spin ½) instead of a three line spectrum of the ^{14}N (nuclear spin 1). The lines of a ^{15}N spectrum are well separated from the ^{14}N lines so that both labels can be used simultaneously in a single experiment (Steinhoff et al. 1991).

Spin labeling by peptide synthesis

A large variety of spin label building blocks (mainly α-, β- and γ-amino acids) for Boc- or Fmoc-based step-by-step peptide synthesis either on a solid support (SPPS) (Merrifield, 1963) or in solution have been synthesized during recent years (Barbosa et al. 1999b; Elsässer et al. 2005). The paramagnetic α-amino acid TOAC (4-amino-1-oxyl-2,2,6,6,-tetramethyl-piperidine-4-carboxylic acid) (Rassat and Rey 1967) is by far the most popular one. It is characterized by only one degree of freedom, the conformation of the six-membered ring (Fig. 2a, b), because the nitroxide is rigidly coupled to the peptide backbone, thereby providing the possibility to obtain direct information about the orientation of secondary structure elements. It has been used to study the secondary structure of small peptides in liquid solution (Anderson et al. 1999; Hanson et al. 1996a; Hanson et al. 1996b; Marsh et al. 2007) and has also been successfully incorporated into the α-melanocyte stimulating hormone without loss of function (Barbosa et al. 1999a). However, a recent study suggests that α-helical structures might be distorted due to the presence of the rigid spin-labeled amino acid (Elsässer et al. 2005). Several N-Boc-protected paramagnetic amino acids with side chains of different polarities and flexibilities have been

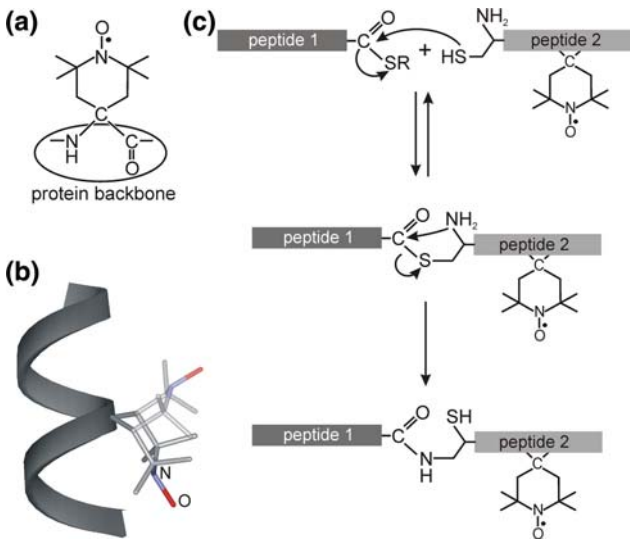

Fig. 2 **a** TOAC amino acid spin label. *Upper panel*: chemical structure. *Bottom panel*: three-dimensional structure of the spin label incorporated into an α-helix. **b** The flip of the six-membered ring as the only possible degree of freedom is shown in *shaded representation*. **c** Native and expressed protein ligation (IPL, EPL). The chemical ligation occurs between a C-terminal thioester (peptide 1) and a sulfhydryl group of an N-terminal Cysteine (peptide 2). After rearrangement through an N → S acyl shift, a peptide bond is formed

synthesized using O′Donnell synthesis (Balog et al. 2003; Balog et al. 2004; O'Donnell et al. 1989).

In general, the chemical synthesis of proteins with incorporated unnatural spin-labeled amino acids relies on the ability to produce the constituent peptides, typically by SPPS. Although the synthesis of polypeptides consisting of up to 166 amino acids (Becker et al. 2003; Kochendoerfer et al. 2003) has become possible through improvements in peptide chemistry, the incorporation of spin-labeled amino acids is still challenging due to the delicate nature of the nitroxide moiety. As, for instance, the nitroxide can be readily protonated under acidic conditions, synthesis conditions have to be identified which are chemically compatible in terms of retaining the oxidation state of the nitroxide group. In case of TOAC, this problem could be overcome by employing Fmoc-based synthesis strategies either on the solid phase in combination with HF cleavage or in solution (Marchetto et al. 1993; Monaco et al. 1999). New strategies for the incorporation of pyrroline-based nitroxide amino acids into polypeptides during SPPS have recently been successfully conducted. In addition, a pyrroline nitroxide spin label has been successfully coupled to the ε-amino group of a selected lysine after complete assembly of the peptide, yielding a paramagnetic stable compound (Becker et al. 2005).

Aiming at the incorporation of spin labels into large proteins, especially membrane proteins, SPPS has to be combined with recombinant techniques. The expressed

protein ligation (EPL), also named intein-mediated protein ligation (IPL), technique can be used to semisynthesize proteins from recombinant and synthetic fragments, thereby extending the size and complexity of the protein targets. The underlying chemical ligation of two polypeptide fragments requires an N-terminal cysteine on one and a C-terminal thioester moiety on the other fragment. After rearrangement through an S → N acyl shift, a native peptide bond is formed (Fig. 2c). The reaction can be performed also in the presence of other unprotected cysteine residues because of a reversible reaction preceding an irreversible step. Using this methodology, a spin-labeled Ras binding domain (RBD) has been synthesized, showing a stable paramagnetic center detected by EPR (Becker et al. 2005).

Spin labeling using the nonsense suppressor methodology

Spin-labeled amino acids have been incorporated in proteins by employing nonsense suppressor methodology, e.g., by utilizing the amber suppressor tRNA chemically aminoacylated with the desired spin label amino acid (Cornish et al. 1994; Mendel et al. 1995; Shafer et al. 2004). Although this strategy might prove generally applicable in the future using unique transfer RNA(tRNA)/aminoacyl–tRNA-synthetase pairs (Chin et al. 2003), only few laboratories are currently equipped to apply this methodology successfully.

Spin labeling with "click chemistry"

As introduced by Kolb, Finn, and Sharpless in 2001 (Kolb et al. 2001), the basic concept of "click chemistry" is the highly selective formation of a carbon–heteroatom bond under mild conditions with high yield. Its modular concept renders it a favorable tool for introducing labels into biomolecules. An example is the 1,3-dipolar cycloaddition of organic azides with alkynes in the presence of Cu(I) (copper-catalyzed azide-alkyne 1,3-dipolar cycloaddition–CuAAC) which has been used to attach fluorescent probes to biomolecules (Deiters and Schultz 2005). Recently, Kalai and coworkers (Kalai et al. 2009) described the synthesis of nitroxide moieties suitable for click chemistry, thereby opening this approach also for site-directed spin labeling.

Spin labeling of nucleic acids

For spin labeling of DNA or RNA, mainly two different approaches are applied. Chemically synthesized nucleotide analogs are used in standard oligonucleotide synthesis. For instance, the spin-labeled thymidine analog (a methyl group replaced by an acetylene-tethered nitroxide Fig. 3a) can be incorporated into deoxyoligonucleotides by using automated phosphite triester methods (Spaltenstein et al. 1988; Spaltenstein et al. 1989). The second approach utilizes nucleotide analogs chemically modified with reactive groups suitable for postsynthetic modification with a spin-labeled reagent. 4-thiouridine derivatives, e.g., can be modified with methanethiosulfonate nitroxide reagents as depicted in Fig. 3b (Qin et al. 2003). A similar approach is the reaction of 2,2,5,5-tetramethyl-pyrrolin-1-xylol-3-acetylene (TPA) with 5-iodo-derivatisized nucleotides through a palladium-catalyzed Sonogashira cross-coupling subsequent to solid-phase synthesis on the solid support (Piton et al. 2005; Piton et al. 2007; Schiemann et al. 2007).

Alternatively, the spin label can be attached to the sugar moiety of specific nucleotides. An example is the

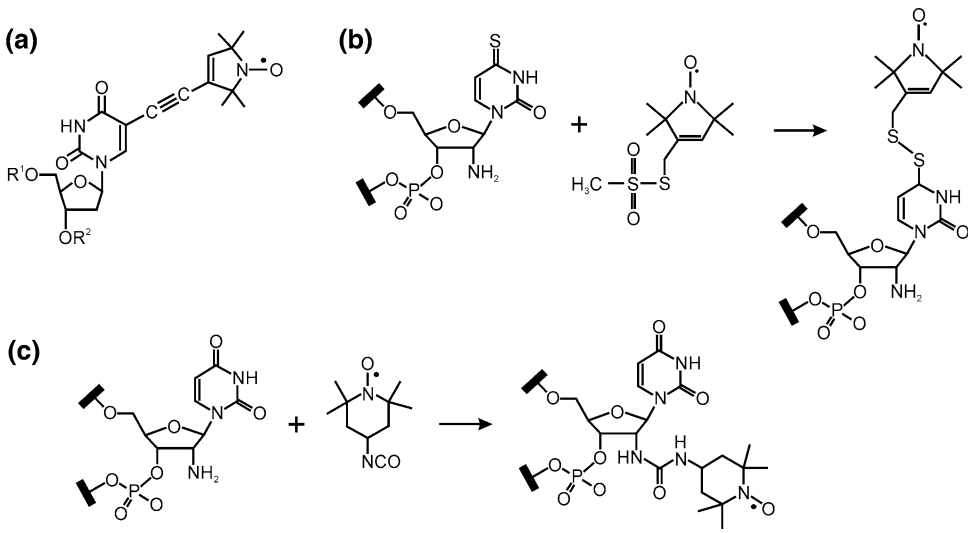

Fig. 3 Spin labeling of nucleic acids. **a** Nitroxide spin-labeled thymidine analog. **b** Modification of 4-thiouridine with MTSSL. **c** Modification of the sugar moiety of nucleotides; postsynthetic derivatization of a 2′-amino group introduced into oligonucleotides with the chemically reactive isocyanate derivative of a TEMPO-like moiety (figure modified according to Edwards et al. 2001)

postsynthetic derivatization of a 2′-amino group introduced into oligonucleotides with a chemically reactive isocyanate derivative of a TEMPO-like moiety (Edwards et al. 2001; Kim et al. 2004), which has been used in pulse EPR-based distance determinations within double stranded DNA model systems (Ward et al. 2007) (see Fig. 3c) as well as in RNA systems, e.g., for an investigation of the dynamics of the trans-activation responsive region (TAR) of HIV RNA (Edwards et al. 2001) or the dynamics of the hammerhead ribozyme (Edwards and Sigurdsson 2005).

EPR analysis of spin-labeled membrane proteins

In the following, the potential of site-directed spin labeling and EPR spectroscopy is exemplified with two model systems: the sensory rhodopsin–transducer complex mediating the photophobic response of the halophilic archaeum *Natronomonas pharaonis* and the photosynthetic reaction center from *Rhodobacter sphaeroides* R26. The photophobic response of the halophilic archaeum *Natronomonas pharaonis* to greenish blue light is mediated by sensory rhodopsin II, NpSRII, which is structurally and functionally closely related to the light-driven proton pump bacteriorhodopsin (for a recent review see Klare et al. 2007). NpSRII comprises seven transmembrane helices (A–G) and a retinal chromophore covalently bound *via* a protonated Schiff base to a conserved lysine residue on helix G. The signal transduction to the intracellular two-component pathway, which modulates the swimming behavior of the cell, is accomplished by the interaction of NpSRII with the tightly bound transducer protein, NpHtrII (halobacterial transducer), in a 2:2 complex. The transducer dimer comprises a transmembrane domain flanked by the two SRII receptors, a linker region consisting of the two so-called HAMP domains (found in histidine kinases, adenylyl cylcases, methyl-accepting chemotaxis proteins, and phosphatases Aravind and Ponting 1999), and a cytoplasmic signaling domain.

The bacterial photosynthetic reaction center, which converts light into chemical energy, has been the subject of intensive research over several decades (Feher 1998). The functional core of the RC is an integral membrane protein complex comprising three subunits (L, M, and H) and ten cofactors, including bacteriochlorophylls (4), bacteriopheophytins (2), quinones (2), a nonheme iron center, and a carotenoid (Feher 2002). This complex catalyzes light-induced charge separation across the membrane, thereby promoting the primary events of photosynthetic energy transduction (Hoff and Deisenhofer 1997).

Nitroxide dynamics

The room temperature EPR spectral shape is sensitive to the reorientational motion of the nitroxide side chain due to partial motional averaging of the anisotropic components of the g- and hyperfine tensors. The influence of the nitroxide dynamics on the spectral shape has been extensively reviewed (Berliner 1976; Berliner 1979; Berliner and Reuben 1989), and its relationship to protein structure has been explored in detail for T4 lysozyme (Mchaourab et al. 1996; Columbus et al. 2001; Columbus and Hubbell 2002). In general, the term nitroxide "mobility" is used to characterize the effects on the EPR spectral features due to the motional rate, amplitude, and anisotropy of the overall reorientational motion of the spin label. For spin-labeled sites exposed to the bulk water, the nitroxide mobility is restricted to a lesser extent, leading to rotational correlation times of the nitroxide in the ns range. The resulting EPR spectra are consequently characterized by small line widths of the center lines, ΔH_0, and small apparent hyperfine splittings. If the mobility of the spin label side chain is restricted by interaction with neighboring side chains or backbone atoms, the line widths and the apparent hyperfine splittings are increased (Fig. 4). For R1 side chains buried in the interior of a protein, as, e.g., for 159R1 of NpSRII, the reorientational motion of the nitroxide is completely

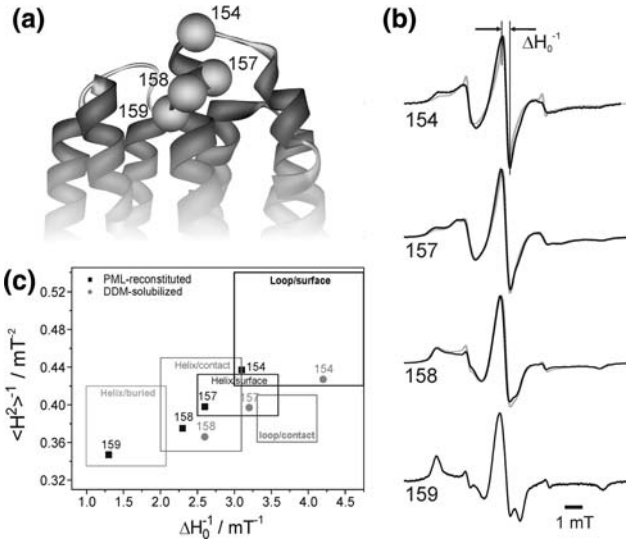

Fig. 4 Mobility analysis of spin labeled proteins. **a** *Ribbon representation* of the NpSRII X-ray structure (Luecke et al. 2001). Cα atoms of spin-labeled sites are depicted as balls (S154R1, K157R1, S158R1, L159R1). **b** X-band EPR spectra of NpSRII solubilized in DDM (*gray*) or reconstituted in purple membrane lipids (*black*). **c** Mobility map. The values of the inverse second moment, $\langle H^2 \rangle^{-1}$, and of the inverse of the central linewidth, ΔH_0^{-1}, of solubilized (*gray circles*) and reconstituted NpSRII (*black squares*) were determined from the spectra shown in panel b. The topological regions of a protein are indicated by boxes according to Isas et al. (2002) and McHaourab et al. (1996)

restricted, and the EPR spectral shape resembles that of a so-called powder spectrum (Fig. 4b). Although the relation between the nitroxide dynamics and spectral line shape is quite complex, the line width of the center line, ΔH_0, and the second moment of the spectra, $\langle H^2 \rangle$, have been found to be correlated with the structure of the binding site environment and have been used as simple semi-empirical mobility parameters (Hubbell et al. 1996; Mchaourab et al. 1996).

For proteins, the plot of these mobility parameters *versus* the residue number reveals secondary structure elements through the periodic variation of the mobility as the nitroxide group sequentially samples surface, tertiary, or buried sites, allowing the assignment of α-helices, β-strands, or random structures. A general classification of regions accommodating buried, surface-exposed, or loop residues can be obtained from the correlation between the inverse of the second moment, $\langle H^2 \rangle^{-1}$, and the inverse of the central line width, ΔH_0^{-1}, as shown in Fig. 4c. Side chains from different topographical regions of a protein can be thereby classified on the basis of the X-ray structures of T4 lysozyme and annexin 12 (Hubbell et al. 1996; Isas et al. 2002; Mchaourab et al. 1996).

For a more quantitative interpretation of the experimental data in terms of dynamic mechanisms and local tertiary interaction, simulations of the EPR spectra have to be performed. On the basis of dynamic models developed by Freed and coworkers (Barnes et al. 1999; Borbat et al. 2001; Freed 1976), excellent agreement of simulations with the corresponding experimental spectra can be obtained. In addition, simulations of ESR spectra can be performed on the basis of molecular dynamics (MD) simulations (Beier and Steinhoff 2006; Budil et al. 2006; DeSensi et al. 2008; Oganesyan 2007; Sezer et al. 2008a; Sezer et al. 2008b; Steinhoff et al. 2000; Steinhoff and Hubbell 1996), providing a direct link between the molecular structure on atomic level and the EPR spectral line shape. This allows to verify, refine, or suggest structural models of spin-labeled proteins based on EPR spectral data.

The viability of MD simulation-based EPR spectra calculation is exemplified with the identification of a spin labeled cysteine side chain in the photosynthetic reaction center (RC) of *Rhodobacter sphaeroides* R26 (Gajula et al. 2007). The RC contains five native cysteines. EPR experiments show that only one cysteine is accessible for spin labeling, either C156 or C234, both located on the H subunit of the RC (Fig. 5a) (Poluektov et al. 2003). EPR spectra calculated from MD simulation trajectories for both candidate positions revealed that only the spin label side chain at position 156 shows a spectrum which is in agreement with the experimental EPR spectrum (see Fig. 5b).

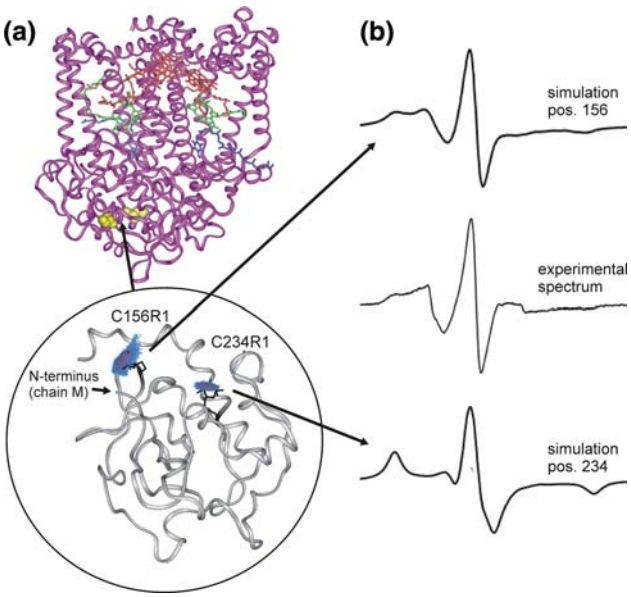

Fig. 5 EPR spectra calculations from MD simulation trajectories for spin-labeled photosynthetic reaction centers from *R. sphaeroides* R26: **a** Structure of the photosynthetic RC (pdb: 1AIJ). The region where the two candidate cysteines are located on subunit F is enlarged (*bottom*), showing the spin label side chains at positions 156 and 234. The conformational space sampled by the spin label side chains during the MD simulation is depicted in blue (low probability to find the NO group of the spin label) and purple (high probability) (Gajula et al. 2007). **b** Experimental (in the *middle*) and calculated EPR spectra, showing that only calculations for a spin label at position 156 (*top*) provide an EPR spectrum which agrees with the experimental one (Gajula et al. 2007)

Solvent accessibilities

The accessibility of the R1 side chain toward paramagnetic probes, which selectively partition in different environments of the system under investigation, can be used to define the location of R1 with respect to the protein/water/membrane boundaries (Fig. 6a). The accessibility of the R1 side chain is defined by its Heisenberg exchange frequency, W_{ex}, with a paramagnetic exchange reagent diffusing in its environment. Metal ion complexes, e.g., NiEDDA or chromium oxalate (CrOx), quantify the accessibility from the bulk water phase. Molecular oxygen or hydrophobic organic radicals, which preferentially partition in the hydrophobic part of the lipid bilayer, define the accessibility of R1 from the lipid phase. For NiEDDA and molecular oxygen, it has been shown that their concentration gradients along the membrane normal can be used to characterize the immersion depth of the spin label side chain with respect to the membrane/water interface (Altenbach et al. 1994; Marsh et al. 2006).

The Heisenberg exchange mechanism leads to variations in the relaxation properties of the spin label attached at the investigated sites, namely, of the spin–lattice relaxation

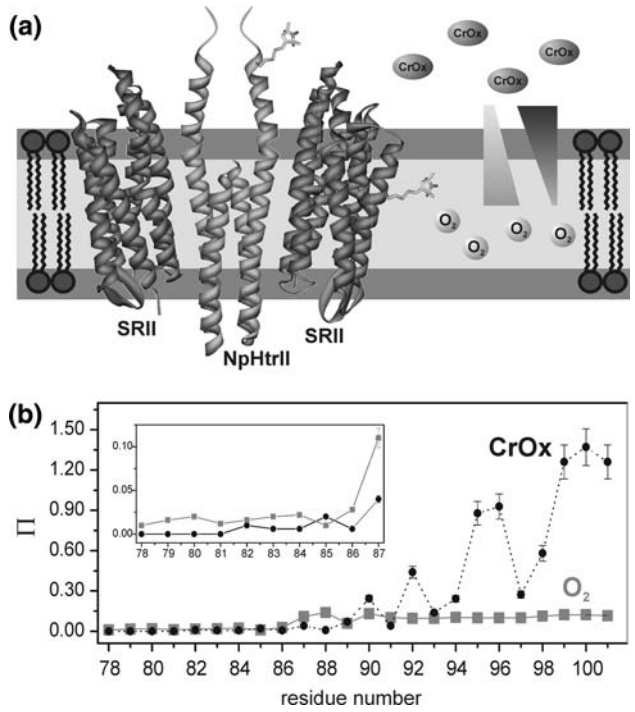

Fig. 6 Solvent accessibilities. **a** *Cartoon representation* of the X-ray structure of the NpSRII/NpHtrII complex (PDB code entry 1H2S Gordeliy et al. 2002) embedded in a lipid bilayer. The NpHtrII structure is extended up to position 96 according to the model based on EPR data (Bordignon et al. 2005). The black and gray triangles indicate the gradient of concentration of the water-soluble reagents (NiEDDA or CrOx) and the lipid-soluble reagent (O_2), respectively. **b** Accessibilities of the R1 side chains of spin-labeled $NpHtrII_{157}$ mutants 78–101 in complex with NpSRII reconstituted in PML. The accessibilities for oxygen (sample in equilibrium with air) and CrOx (50 mM) are depicted in terms of the dimensionless accessibility parameter Π *versus* residue number. The inset shows a magnification of the region from position 78–87 for better visualization of the periodical accessibility pattern due to the helical structure

time T_{1e} and the spin–spin relaxation time T_{2e}. Thereby, if the longitudinal relaxation time of the reagent is smaller than the encounter complex lifetime ($T_{1R} < \tau_c$), the Heisenberg exchange leads to equal changes in T_{1e} and T_{2e}:

$$W_{ex} = \Delta\left(\frac{1}{T_{1e}}\right) = \Delta\left(\frac{1}{T_{2e}}\right) = k_c C_R$$

where k_{ex} is the exchange constant and C_R is the concentration of the paramagnetic exchange reagent (R). Several methods can be applied to determine the Heisenberg exchange frequency, W_{ex}. Most commonly, exchange rates for nitroxide side chains in proteins are measured using cw power saturation, where the EPR signal amplitude is monitored as a function of the incident microwave power in the absence and presence of the paramagnetic quencher. From the saturation behavior of the nitroxide, the widely used dimensionless "accessibility parameter", Π, can be extracted, which is proportional to W_{ex} (Altenbach et al. 1989a; Altenbach et al. 2005; Farahbakhsh et al. 1992). Alternatively, W_{ex} can be determined directly from the change of the spin–lattice relaxation time, T_{1e}, on the addition of the quencher, where T_{1e} is measured by pulse EPR methods (Altenbach et al. 2005; Altenbach et al. 1989b; Feix et al. 1984; Mchaourab and Hyde 1993; Nielsen et al. 2004; Pyka et al. 2005; Shin and Hubbell 1992; Yin et al. 1987). The water accessibility can also be determined by electron spin echo envelope modulation spectroscopy in the presence of deuterated water and by deuterium contrast in transversal relaxation rates. As shown for different residues in major plant light-harvesting complex IIb, a systematic comparison of these parameters allows for a detailed characterization of the environment of the spin-labeled residues (Volkov et al. 2009).The value of an accessibility analysis is exemplified with a segment of the transducer protein NpHtrII associated with its cognate photoreceptor receptor NpSRII reconstituted in purple membrane lipids (Fig. 6b) (Bordignon et al. 2005). The accessibility data were obtained for 20 spin-labeled samples with the R1 side chains located at the end of TM2, positions 78–82 (for which X-ray data are available) and in the AS-1 sequence of the HAMP domain, positions 83–101 (for which no structural information is available). The low Π values found for both CrOx and O_2 for positions 78–86 indicate residues in a densely packed protein–protein interface, corroborating the low mobility values measured for the same region. The periodicity of 3.6 residues revealed by the oxygen accessibility from positions 78 to 89 strongly supports the assumption that this part of the AS-1 sequence is an α-helical extension of TM2. For positions 87 to 94, the accessibility values for the water soluble quencher CrOx gradually increase in line with the notion that the side chains become more exposed to the bulk water. A similar increase in the spin label mobility is also observed. This provides strong evidence that the region 87–94 of the transducer is protruding out of the protein–protein interface into the cytoplasm. Accordingly, the accessibility values for O_2 also increase. The periodicity observed in this region cannot be clearly correlated with a helical pattern, although it might be present. The following positions 95 to 101 exhibit CrOx accessibility values resembling those for residues exposed to the bulk water.

Polarity of the nitroxide microenvironment

Polarity and proticity of the spin label microenvironment are reflected in the hyperfine component A_{zz} and the g tensor component g_{xx}. In general, a polar environment shifts A_{zz} to higher values, whereas the tensor component g_{xx}, as determined from the B-field of the canonical peak position ($g_{xx} = h\nu/\mu_B B$), is decreased (cf. Fig. 7). The A_{zz}

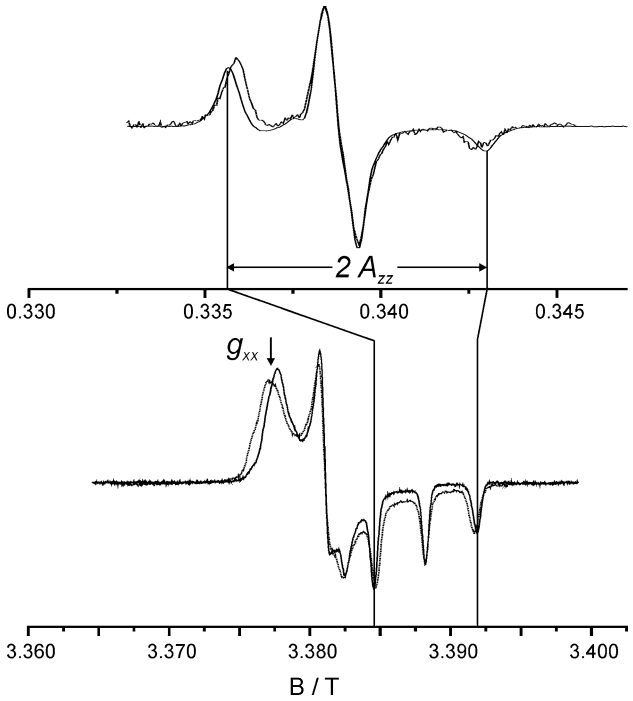

Fig. 7 Comparison of X-(∼9.5 GHz, *top*) and W-band (∼95 GHz, *bottom*) spectra, determined at 160 K, of the spin labeled NpSRII mutants V17R1 (*dotted line*) and L89R1 (*solid line*), showing different g_{xx} and A_{zz} values. The lower polarity of the micro-environment of V17R1, which is embedded in the lipid bilayer, compared to L89R1, which is located at the cytoplasmic surface, is obvious from the significantly reduced A_{zz} value and the increase in g_{xx}. The spectral features representing A_{zz} in the X- and W-band spectra of L89R1 are connected by lines

component can be obtained from cw X-band ESR spectra of spin-labeled proteins in frozen samples, whereas the principal g-tensor components and their variation can be determined with high accuracy using high-field EPR techniques due to the enhanced Zeeman resolution of rigid-limit spectra of disordered samples (Huber and Törring 1995; Steinhoff et al. 2000b). Figure 7 shows a comparison of X- and W-band spectra for the R1 side chain in a polar (NpSRII L89R1) and in an apolar (NpSRII V17R1) environment. In regular secondary structure elements with anisotropic solvation as, e.g., surface exposed α-helices, the water density and, hence, the tensor component values A_{zz} and g_{xx} follow a periodic function of residue number. These data can be used similarly to the accessibility data determined for water-soluble paramagnetic exchange reagents (see section "Solvent accessibilities") to obtain structural and topological information. In addition, the polarity of the spin label environment can reveal detailed information on the protein fold.

As an example, the polarity parameter values for the sequence 88–94 in the first HAMP domain of NpHtrII in complex with NpSRII are plotted in Fig. 8a (Plato et al. 2002; Brutlach et al. 2006). From these data, it is evident that positions 90 and 93 of NpHtrII are located in a more polar, water-accessible environment, as is the position 154 on the cytoplasmic surface of NpSRII. In contrast, positions 88, 89, 91, 92, and 94 reside in a more apolar environment, less accessible to water. Also evident from the polarity plot is a periodical pattern, corroborating the α-helical structure of this region. The exceptional apolar character of the position 78 indicates that this side chain is deeply buried in a protein–protein or protein–lipid interface. These experimental results are reflected in the structural model which has been based in addition on mobility, accessibility and distance data (Bordignon et al. 2005) for this region (Fig. 8b and c). Residues 88, 91, and 92 are located in protein–protein interfaces, whereas positions 90 and 93 are positioned at the opposite side of

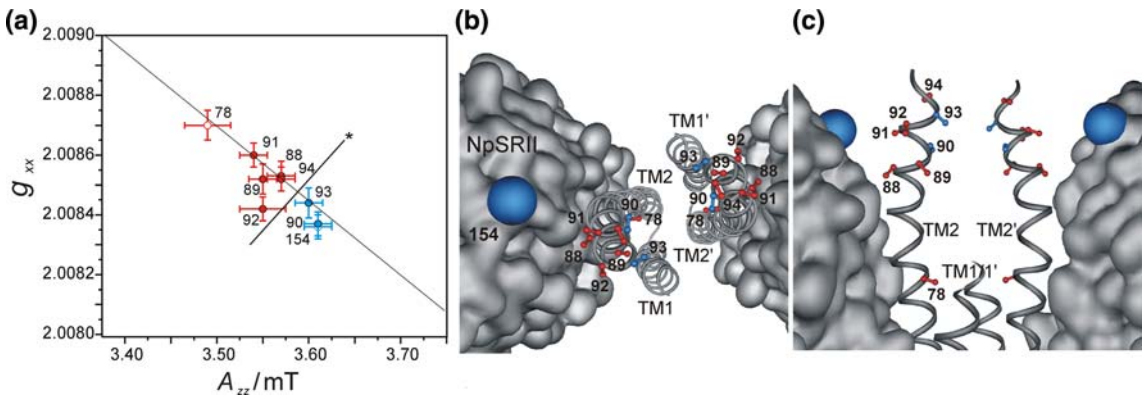

Fig. 8 **a** Plot of g_{xx} versus A_{zz} of R1for positions 88–94 in NpHtrII according to the data published by Brutlach et al. 2006. The plot also includes values for position 78 on the second transmembrane helix (TM2) and for position 154 in NpSRII. An arbitrary threshold of g_{xx}/A_{zz} indicated by the diagonal line marked with * classifies the sites into more polar (*blue*) or more apolar sites (*red*). **b** View from the cytoplasm onto the NpSRII moieties (*surface representation*) and the four-helix bundle of the transducer (*ribbon representation*) up to position 96 according to the EPR model (Bordignon et al. 2005). Residues 78 and 88-94 in NpHtrII are highlighted. **c** Side view of the NpSRII-NpHtrII complex structure

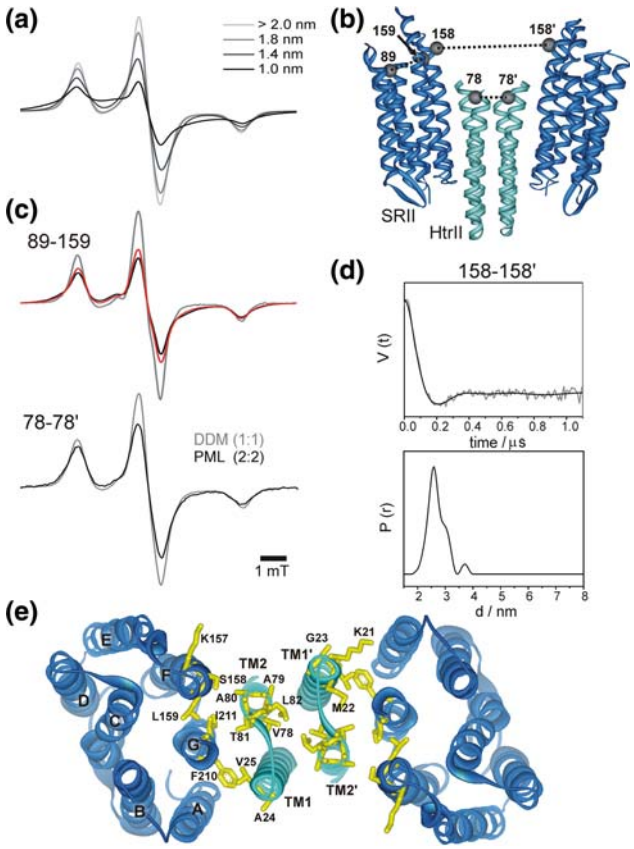

Fig. 9 Interspin distance measurements. **a** Simulated powder spectra (normalized to constant spin number) for different interspin distances. The parameters used are $g_{xx} = 2.0086$, $g_{yy} = 2.0066$, $g_{zz} = 2.0026$, $A_{xx} = 0.52$ mT, $A_{yy} = 0.45$ mT, and $A_{zz} = 3.5$ mT. The spectra were convoluted with a field-independent line shape function composed of a superposition of 44% Lorentzian and 56% Gaussian- of 0.33 and 0.39-mT width, respectively, and a fraction of a singly spin-labeled component of 30%. **b** *Ribbon representation* of the X-ray structure of the 2:2 NpSRII–NpHtrII complex (PDB 1H2S). Cβ atoms of L89R1, S158R1 and L159R1 in NpSRII, and V78R1 in NpHtrII, are shown as spheres. **c** (*top*) Cw EPR spectra ($T = 160$ K) of the double mutant NpSRII–L89R1/L159R1 in the receptor ground state (*black*) and in the trapped signaling state (M-state, *red*). Comparison with the sum of the spectra of the singly labeled samples (*grey*) reveals line broadening due to dipolar interaction. Interspin distances of 1.1 ($\pm$0.2) nm for the ground state and 1.3 ($\pm$0.2) nm for the M-trapped state (assuming 100% yield of the trapping procedure) have been determined (data taken from Bordignon et al. 2007); (*bottom*) $NpHtrII_{157}$–V78R1 solubilized in DDM (*gray*) or reconstituted in PML (*black*) in the absence of NpSRII. The interspin distance obtained in the reconstituted sample is 1.3 ($\pm$0.2) nm; the fraction of the singly labeled species amounts to 57% (data taken from Klare et al. 2006). **d** (*upper panel*) DEER time domain data obtained after division by the background for NpSRII-S158R1. The distance distribution shown in the bottom panel is obtained by Tikhonov regularization using the Software Deer Analysis 2008 (Jeschke et al. 2006) with a regularization parameter of 10. The mean distance of 2.6 nm between the two nitroxides bound to positions 158 in the 2:2 complex is in good agreement with the distance of 3 nm between the oxygen atoms of the respective serine residues as calculated from the crystal structure. **e** EPR model of the transmembrane region of the receptor–transducer complex (Wegener et al. 2001). Receptor helices are shown as blue, and transducer helices as cyan ribbons. Side chains, which were replaced by cysteines and spin labeled for interspin distances measurements, are shown in *stick shaped representation*

the transducer helix. The position 78 is, in line with the exceptional low polarity of its micro-environment, buried in the densely packed four helix bundle comprised by the NpHtrII dimer.

Intra- and intermolecular distance determination

The distance between the two spin label side chains introduced into a protein can be determined through quantification of their spin–spin interaction, thus providing valuable structural information. Spin–spin interaction is composed of static dipolar interaction, modulation of the dipolar interaction by the residual motion of the spin label side chains, and exchange interaction. The static dipolar interaction in an unordered, immobilized sample leads to considerable broadening of the cw EPR spectrum if the interspin distance is <2 nm (Fig. 9a, c). Interspin distances can then be quantified by a detailed line shape analysis of EPR spectra of frozen protein samples or proteins in solutions of high viscosity using spectra convolution or deconvolution techniques (Altenbach et al. 2001; Rabenstein and Shin 1995; Steinhoff et al. 1991; Steinhoff et al. 1997). Recent advances in pulse EPR techniques expanded the accessible distance range up to 8 nm (Borbat and Freed 1999; Pannier et al. 2000). Two major protocols have been successfully applied, the 4-pulse DEER or 4-pulse PELDOR (see Fig. 9b) and the Double Quantum Coherence approaches (for a recent review see Schiemann and Prisner 2007). The combination of cw and pulse EPR techniques, taking into account borderline effects in the region of 1.6 to 1.9 nm (Banham et al. 2008; Grote et al. 2008), provides means to determine interspin distances in the range of 1 to 8 nm, thereby covering the most important distance regime necessary for structural investigations on biomacromolecules.

Based on interspin distances determined for 26 different pairs of spin label side chains introduced into the cytoplasmic moieties of NpSRII and NpHtrII, e.g., the arrangement of the transmembrane domains of this complex was modeled (Wegener et al. 2001) (Fig. 9e). Direct comparison of the EPR model with the latter determined crystal structure (Gordeliy et al. 2002) (see Fig. 11b) emphasizes the consistency of the EPR model with that of the X-ray structure, especially, if the general topology, the location, and the relative orientation of the transmembrane helices are considered. Notably, most of the side-chain orientations within the complex coincide quite well in the two models, although in the EPR model the bacteriorhodopsin structure had to be used as a

template for NpSRII, since the NpSRII structure was not known. In a subsequent study, it was shown that the structural properties of the HAMP domain as proven by mobility, accessibility, and intra-transducer–dimer distance data are in agreement with the four helical bundle NMR models of the HAMP domain from *Archaeoglobus fulgidus* (Döbber et al. 2008).

The interspin distance determination between a nitroxide and a native cofactor in its paramagnetic state by DEER is exemplified with the semiquinone anion state of the primary acceptor (Q_A) and a spin label at the native cysteine C156 in the H subunit of the photosynthetic reaction center from *Rhodobacter sphaeroides* R26 (Fig. 10) (Borovykh et al. 2006). The dipolar evolution trace of a sample kept in the dark does not show any modulation due to the fact that Q_A is not in its paramagnetic state (Fig. 10b). The illuminated sample clearly exhibits modulation of the echo signal due to the presence of the paramagnetic semiquinone in close proximity to the spin label side chain. Analysis of the data reveals a Gaussian-shaped distance distribution with an average interspin distance of 3.05 nm between Q_A and the spin label (Fig. 10c). MD simulations based on the crystal coordinates of RC as the starting structure result in an average distance deviating by approximately 10% from that of the experiment which was attributed to possible difference of the RC conformation in the crystal and in solution, or due to the replacement of the native Fe(II) by Zn(II) (Borovykh et al. 2006).

Interspin distances between paramagnetic metal ions and spin label side chains have been determined by

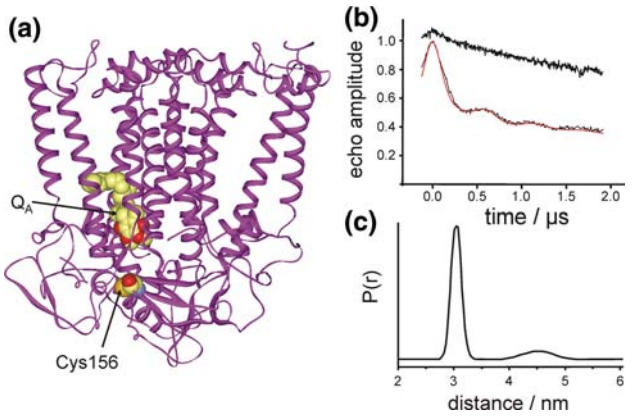

Fig. 10 Distance determination between a native cofactor and a spin label in the reaction center of *R. sphaeroides* (Borovykh et al. 2006): **a** Crystal structure (*ribbon representation*, pdb: 1AIJ) of the photosynthetic RC showing the positions of Q_A and the spin labeled cysteine at position 156 in *space-fill ed representation*. **b** Dipolar evolution traces of the DEER experiments with the sample in the dark (*top*) and on illumination (*bottom*); The red line represents the fit with the Gaussian distance distribution shown in (**c**)

analysis of the EPR line width of the spin label spectrum based on a theory of Leigh (1970) (this methodology has been extensively reviewed in e.g. Berliner et al. 2000), and in a very recent approach by the use of PELDOR techniques (Bode et al. 2008). Remarkably, the PELDOR traces contain, besides the distance information, also information about the orientation of the paramagnetic centers, their conformational flexibility, and the spin density distribution, thereby increasing the amount and quality of data for a setup or verification of structural models. Another recent approach utilizes the modulation of the relaxation rates by dipolar interaction to determine the distance between the iron center and a spin label side chain introduced into metmyoglobin (Zhou et al. 2000), and the enhancement of longitudinal relaxation of a nitroxide label due to a lanthanide complex label (Jäger et al. 2008). In the latter study, the relaxivity of a dysprosium complex with the macrocyclic ligand DOTA was determined without direct measurements of longitudinal relaxation rates of the lanthanide by analyzing the dependence of relaxation enhancement on either temperature or concentration in homogeneous glassy frozen solutions, revealing a distance of about 2.7 nm in a model compound of the type nitroxide–spacer–lanthanide complex.

Time-resolved detection of conformational changes

Conformational changes of proteins can be followed in time by monitoring any of the parameters discussed above with up to 100 µs resolution using conventional EPR instrumentation and detection schemes (field modulation). Examples found in the literature are the detection of helix motions in rhodopsin, bacteriorhodopsin (Altenbach et al. 2008; Farahbakhsh et al. 1993; Farrens et al. 1996; Steinhoff et al. 1994; Thorgeirsson et al. 1997), and sensory rhodopsin II (Bordignon et al. 2007). Light-induced conformational changes in the NpSRII–NpHtrII complex as detected by SDSL EPR are shown in Fig. 11. The change of interspin distances measured, between different spin-labeled sites in NpSRII and NpHtrII in the dark and in the frozen M state, revealed a light-induced outward tilt of helix F, which leads to a transient rotation of helix TM2 in the transducer (Bordignon et al. 2007; Klare et al. 2004; Wegener et al. 2000; Wegener et al. 2001). The light-induced outward movement of the cytoplasmic moiety of helix F leads to a transient decrease of the nitroxide motional restrictions at position 159. Concomitantly, the EPR signal of V78R1 in TM2 changes due to the decrease of the dipolar coupling between V78R1 and V78'R1 in the transducer dimer. Comparison of the EPR transient changes with the optical traces recorded at different wavelengths allow to identify the M state as the signaling state where the observed

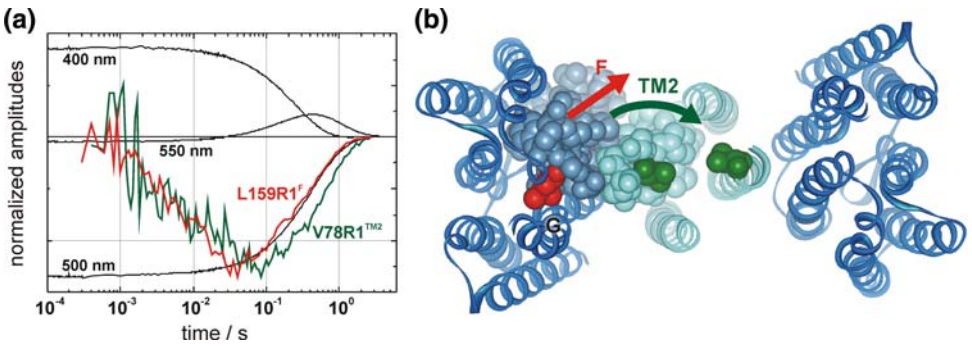

Fig. 11 Conformational changes of the NpSRII–NpHtrII complex followed by EPR spectroscopy. **a** View from the cytoplasm onto the NpSRII–NpHtrII complex, illustrating light-induced conformational changes of the receptor helix F and the transducer helix TM2 as derived from EPR data. The *space-filled representation* shows the tight interaction between helix F and TM2. The light-induced outward tilt of helix F (*red arrow*) drives TM2 into a clockwise rotation (*green arrow*). **b** Light-induced EPR signal changes (*noisy lines*) and the corresponding optical traces (*continuous lines*) recorded at 500 nm (*ground state*), 550 nm (O state), and 400 nm (M state) of NpSRII–NpHtrII reconstituted in PML ($T = 293$ K) (Klare et al. 2004). The EPR transients for NpSRII–L159R1 (*red*) and NpSRII–NpHtrIIV78R1 (*green*) were recorded at fixed B-field values, where light-induced spectral changes reveal a maximum. The structural rearrangements in NpSRII and in NpHtrII occur synchronously with a time constant of ~3 ms. The back reaction in NpSRII follows the recovery of the ground state, but it is delayed for NpHtrII

conformational changes occur. With the reformation of the ground state, the reaction of the receptor seems to be decoupled from that of the transducer. The transient rotation of TM2 in the transmembrane region of the protein causes rotation of the extension of this helix within the HAMP domain, which in turn could shift the recently unraveled equilibrium between two HAMP conformations toward the on or off states, thus eliciting the signal transfer (Döbber et al. 2008).

References

Altenbach C, Flitsch SL, Khorana HG, Hubbell WL (1989a) Structural studies on transmembrane proteins. 2. Spin labeling of bacteriorhodopsin mutants at unique cysteines. Biochemistry 28:7806–7812

Altenbach C, Froncisz W, Hyde JS, Hubbell WL (1989b) Conformation of spin-labeled melittin at membrane surfaces investigated by pulse saturation recovery and continuous wave power saturation electron paramagnetic resonance. Biophys J 56:1183–1191

Altenbach C, Marti T, Khorana HG, Hubbell WL (1990) Transmembrane protein structure: spin labeling of bacteriorhodopsin mutants. Science 248:1088–1092

Altenbach C, Greenhalgh DA, Khorana HG, Hubbell WL (1994) A collision gradient method to determine the immersion depth of nitroxides in lipid bilayers: application to spin-labeled mutants of bacteriorhodopsin. Proc Natl Acad Sci USA 91:1667–1671

Altenbach C, Oh KJ, Trabanino RJ, Hideg K, Hubbell WL (2001) Estimation of inter-residue distances in spin labeled proteins at physiological temperatures: experimental strategies and practical limitations. Biochemistry 40:15471–15482

Altenbach C, Froncisz W, Hemker R, Mchaourab H, Hubbell WL (2005) Accessibility of nitroxide side chains: absolute Heisenberg exchange rates from power saturation EPR. Biophys J 89:2103–2112

Altenbach C, Kusnetzow AK, Ernst OP, Hofmann KP, Hubbell WL (2008) High-resolution distance mapping in rhodopsin reveals the pattern of helix movement due to activation. Proc Natl Acad Sci USA 105:7439–7444

Anderson DJ, Hanson P, McNulty J, Millhauser GL, Monaco V, Formaggio F et al (1999) Solution structures of TOAC-labeled trichogin GA IV peptides from allowed (g = 2) and half-field electron spin resonance. J Am Chem Soc 121:6919–6927

Aravind L, Ponting CP (1999) The cytoplasmic helical linker domain of receptor histidine kinase and methyl-accepting proteins is common to many prokaryotic signalling proteins. FEMS Microbiol Lett 176:111–116

Balog M, Kalai T, Jeko J, Berente Z, Steinhoff H-J, Engelhard M, Hideg K (2003) Synthesis of new conformationally rigid paramagnetic [alpha]-amino acids. Tetrahedron Lett 44:9213–9217

Balog M, Kalai T, Jekö J, Steinhoff H-J, Engelhard M, Hideg K (2004) Synthesis of new 2, 2, 5, 5-tetramethyl-2, 5-dihydro-1H-pyrrol-1-yloxyl radicals and 2-substituted-2, 5, 5-trimethylpyrrolidin-1-yloxyl radicals based a-amino acids. Synlett 14:2591–2593

Banham JE, Baker CM, Ceola S, Day IJ, Grant GH, Groenen EJJ et al (2008) Distance measurements in the borderline region of applicability of CW EPR and DEER: a model study on a homologous series of spin-labelled peptides. J Magn Reson 191:202–218

Barbosa SR, Cilli EM, Lamy-Freund MT, Castrucci AM, Nakaie CR (1999a) First synthesis of a fully active spin-labeled peptide hormone. FEBS Lett 446:45–48

Barbosa SR, Cilli EM, Lamy-Freund MT, Castrucci AM, Nakaie CR (1999b) First synthesis of a fully active spin-labeled peptide hormone. FEBS Lett 446:45–48

Barnes JP, Liang Z, Mchaourab HS, Freed JH, Hubbell WL (1999) A multifrequency electron spin resonance study of T4 lysozyme dynamics. Biophys J 76:3298–3306

Becker CFW, Hunter CL, Seidel R, Kent SBH, Goody RS, Engelhard M (2003) Total chemical synthesis of a functional interacting protein pair: the protooncogene H-Ras and the Ras-binding domain of its effector c-Raf1. Proc Natl Acad Sci USA 100:5075–5080

Becker CFW, Lausecker K, Balog M, Kalai T, Hideg K, Steinhoff H-J, Engelhard M (2005) Incorporation of spin-labelled amino acids into proteins. Magn Reson Chem 43:S34–S39

Beier C, Steinhoff H-J (2006) A structure-based simulation approach for electron paramagnetic resonance spectra using molecular and stochastic dynamics simulations. Biophys J 91:2647–2664

Berliner LJ (ed) (1976) Spin labeling: theory and applications. Academic Press, New York

Berliner LJ (ed) (1979) Spin labeling II: theory and applications. Academic Press, New York

Berliner LJ, Reuben J (eds) (1989) Spin labeling theory and applications. Plenum Press, New York

Berliner LJ, Grunwald J, Hankovszky HO, Hideg K (1982) A novel reversible thiol-specific spin label: papain active site labeling and inhibition. Anal Biochem 119:450–455

Berliner LJ, Eaton SS, Eaton GR (eds) (2000) Distance measurements in biological systems by EPR. New York, Plenum Press

Bode BE, Plackmeyer J, Prisner TF, Schiemann O (2008) PELDOR measurements on a nitroxide-labeled Cu(II) porphyrin: orientation selection, spin-density distribution, and conformational flexibility. J Phys Chem A 112:5064–5073

Borbat PP, Freed JH (1999) Multiple-quantum ESR and distance measurements. Chem Phys Lett 313:145–154

Borbat PP, Costa-Filho AJ, Earle KA, Moscicki JK, Freed JH (2001) Electron spin resonance in studies of membranes and proteins. Science 291:266–269

Bordignon E, Steinhoff H-J (2007) Membrane protein structure and dynamics studied by site-directed spin labeling ESR. In: Hemminga MA, Berliner LJ (eds) ESR spectroscopy in membrane biophysics. Springer Science and Business Media, New York, pp 129–164

Bordignon E, Klare JP, Döbber MA, Wegener AA, Martell S, Engelhard M, Steinhoff H-J (2005) Structural analysis of a HAMP domain: the linker region of the phototransducer in complex with sensory rhodopsin II. J Biol Chem 280:38767–38775

Bordignon E, Klare JP, Holterhues J, Martell S, Krasnaberski A, Engelhard M, Steinhoff H-J (2007) Analysis of light-induced conformational changes of *Natronomonas pharaonis* sensory rhodopsin II by time resolved electron paramagnetic resonance spectroscopy. Photochem Photobiol 83:263–272

Borovykh IV, Ceola S, Gajula P, Gast P, Steinhoff H-J, Huber M (2006) Distance between a native cofactor and a spin label in the reaction centre of *Rhodobacter sphaeroides* by a two-frequency pulsed electron paramagnetic resonance method and molecular dynamics simulations. J Magn Res 180:178–185

Brutlach H, Bordignon E, Urban L, Klare JP, Reyher H-J, Engelhard M, Steinhoff H-J (2006) High-field EPR and site-directed spin labeling reveal a periodical polarity profile: the sequence 88 to 94 of the phototransducer, NpHtrII, in complex with sensory rhodopsin, NpSRII. Appl Magn Reson 30:359–372

Budil DE, Sale KL, Khairy K, Fajer PG (2006) Calculating slow-motional electron paramagnetic resonance spectra from molecular dynamics using a diffusion operator approach. J Phys Chem A 110:3703–3713

Chin JW, Cropp TA, Anderson JC, Mukherji M, Zhang Z, Schultz PG (2003) An expanded eukaryotic genetic code. Science 301:964–967

Columbus L, Hubbell WL (2002) A new spin on protein dynamics. Trends Biochem Sci 27:288–295

Columbus L, Tamas K, Jekö J, Kalman H, Hubbell WL (2001) Molecular motion of spin labeled side chains in a-helices: analysis by variation of side chain structure. Biochem 40:3828–3846

Cornish VW, Benson DR, Altenbach C, Hideg K, Hubbell WL, Schultz PG (1994) Site-Specific incorporation of biophysical probes into proteins. Proc Natl Acad Sci USA 91:2910–2914

Deiters A, Schultz PG (2005) In vivo incorporation of an alkyne into proteins in Escherichia coli. Bioorg Med Chem Lett 15:1521–1524

DeSensi SC, Rangel DP, Beth AH, Lybrand TP, Hustedt EJ (2008) Simulation of nitroxide electron paramagnetic resonance spectra from Brownian trajectories and molecular dynamics simulations. Biophys J 94:3798–3809

Döbber MA, Bordignon E, Klare JP, Holterhues J, Martell S, Mennes N et al (2008) Salt-driven equilibrium between two conformations in the HAMP domain from *Natronomonas pharaonis*: the language of signal transfer? J Biol Chem 283:28691–28701

Edwards TE, Sigurdsson ST (2005) EPR spectroscopic analysis of U7 hammerhead ribozyme dynamics during metal ion induced folding. Biochem 44:12870–12878

Edwards TE, Okonogi TM, Robinson BH, Sigurdsson ST (2001) Site-specific incorporation of nitroxide spin-labels into internal sites of the TAR RNA; structure-dependent dynamics of RNA by EPR spectroscopy. J Am Chem Soc 123:1527–1528

Elsässer C, Monien B, Haehnel W, Bittl R (2005) Orientation of spin labels in de novo peptides. Magn Reson Chem 43:S26–S33

Farahbakhsh ZT, Altenbach C, Hubbell WL (1992) Spin labeled cysteines as sensors for protein–lipid interaction and conformation in rhodopsin. Photochem Photobiol 56:1019–1033

Farahbakhsh ZT, Hideg K, Hubbell WL (1993) Photoactivated conformational changes in rhodopsin: a time-resolved spin label study. Science 262:1416–1419

Farrens DL, Altenbach C, Yang K, Hubbell WL, Khorana HG (1996) Requirement of rigid-body motion of transmembrane helices for light activation of rhodopsin. Science 274:768–770

Feher G (1998) Three decades of research in bacterial photosynthesis and the road leading to it: a personal account. Photosynth Res 55:1–40

Feher G (2002) My road to biophysics: picking flowers on the way to photosynthesis. Annu Rev Biophys Biomol Struct 31:1–44

Feix JB, Popp CA, Venkataramu SD, Beth AH, Park JH, Hyde JS (1984) An electron–electron double-resonance study of interactions between [^{14}N]- and [^{15}N]stearic acid spin-label pairs: lateral diffusion and vertical fluctuations in dimyristoylphosphatidylcholine. Biochem 23:2293–2299

Freed JH (1976) Theory of slow tumbling ESR spectra for nitroxides. In: Berliner LJ (ed) Spin labeling: theory and applications. Academic Press, New York, pp 53–132

Gajula P, Borovykh IV, Beier C, Shkuropatova T, Gast P, Steinhoff H-J (2007) Spin-labeled photosynthetic reaction centers from *Rhodobacter sphaeroides* studied by electron paramagnetic resonance spectroscopy and molecular dynamics simulation. Appl Magn Reson 31:167–178

Gordeliy VI, Labahn J, Moukhametzianov R, Efremov R, Granzin J, Schlesinger R et al (2002) Molecular basis of transmembrane signalling by sensory rhodopsin II-transducer complex. Nature 419:484–487

Griffith OH, McConnell HM (1966) A nitroxide-maleimide spin label. Proc Natl Acad Sci USA 55:8–11

Grote M, Bordignon E, Polyhach Y, Jeschke G, Steinhoff HJ, Schneider E (2008) A comparative EPR study of the nucleotide-binding domains' catalytic cycle in the assembled maltose ABC-importer. Biophys J 95:2924–2938

Hanson P, Martinez G, Millhauser G, Formaggio F, Crisma M, Toniolo C, Vita C (1996a) Distinguishing helix conformations in alanine-rich peptides using the unnatural amino acid TOAC and electron spin resonance. J Am Chem Soc 118:271–272

Hanson P, Millhauser G, Formaggio F, Crisma M, Toniolo C (1996b) ESR characterization of hexameric, helical peptides using double TOAC spin labeling. J Am Chem Soc 118:7618–7625

Hoff AJ, Deisenhofer J (1997) Photophysics of photosynthesis. Structure and spectroscopy of reaction centers of purple bacteria. Phys Rep 287:1–247

Hubbell WL, Mchaourab HS, Altenbach C, Lietzow MA (1996) Watching proteins move using site-directed spin labeling. Structure 4:779–783

Hubbell WL, Gross A, Langen R, Lietzow MA (1998) Recent advances in site-directed spin labeling of proteins. Curr Opin Struc Biol 8:649–656

Huber M, Törring JT (1995) High-field EPR on the primary electron donor cation radical in single crystals of heterodimer mutant reaction centers of photosynthetic bacteria—first characterization of the G-tensor. Chem Phys 194:379–385

Isas JM, Langen R, Haigler HT, Hubbell WL (2002) Structure and dynamics of a helical hairpin and loop region in annexin 12: a site-directed spin labeling study. Biochemistry 41:1464–1473

Jäger H, Koch A, Maus V, Spiess HW, Jeschke G (2008) Relaxation-based distance measurements between a nitroxide and a lanthanide spin label. J Magn Res 194:254–263

Jeschke G, Bender A, Schweikardt T, Panek G, Decker H, Paulsen H (2005) Localization of the N-terminal domain in light-harvesting chlorophyll a/b protein by EPR measurements. J Biol Chem 280:18623–18630

Jeschke G, Chechik V, Ionita P, Godt A, Zimmermann H, Banham JE et al (2006) Deer analysis 2006—a comprehensive software package for analyzing pulsed ELDOR data. Appl Magn Reson 30:473–498

Kalai T, Hubbell WL, Hideg K (2009) Click reactions with nitroxides. Synthesis 2009:1336–1340

Kim N-K, Murali A, DeRose VJ (2004) A distance ruler for RNA using EPR and site-directed spin labeling. Chem Biol 11:939–948

Klare JP, Gordeliy VI, Labahn J, Büldt G, Steinhoff H-J, Engelhard M (2004) The archaeal sensory rhodopsin II/transducer complex: a model for transmembrane signal transfer. FEBS Lett 564:219–224

Klare JP, Bordignon E, Döbber MA, Fitter J, Kriegsmann J, Chizhov I et al (2006) Effects of solubilization on the structure and function of the sensory rhodopsin II/transducer complex. J Mol Biol 356:1207–1221

Klare JP, Chizhov I, Engelhard M (2007) Microbial rhodopsins: scaffolds for ion pumps, channels, and sensors. Results Probl Cell Differ 45:73–122

Klug CS, Feix JB (2008) methods and applications of site-directed spin labeling EPR spectroscopy. In: Correia JJ, Detrich HW (eds) Methods in cell biology. Biophysical tools for biologists, volume one: in vitro techniques. New York, Academic Press, pp 617–658

Kochendoerfer GG, Chen SY, Mao F, Cressman S, Traviglia S, Shao H, Hunter CL, Low DW, Cagle EN, Carnevali M, Gueriguian V, Keogh PJ, Porter H, Stratton SM, Wiedeke MC, Wilken J, Tang J, Levy JJ, Miranda LP, Crnogorac MM, Kalbag S, Botti P, Schindler-Horvat J, Savatski L, Adamson JW, Kung A, Kent SB, Bradburne JA (2003) Design and chemical synthesis of a homogeneous polymer-modified erythropoiesis protein. Science 299:884–887

Kolb H, Finn MG, Sharpless KB (2001) Click chemistry: diverse chemical function from a few good reactions. Angew Chem Int Ed Engl 40:2004–2021

Leigh JS Jr (1970) ESR rigid-lattice line shape in a system of two interacting spins. J Chem Phys 52:2608–2612

Luecke H, Schobert B, Lanyi JK, Spudich EN, Spudich JL (2001) Crystal structure of sensory rhodopsin II at 2.4 A: insights into color tuning and transducer interaction. Science 293:1499–1503

Marchetto R, Schreier S, Nakaie CR (1993) A novel spin-labeled amino-acid derivative for use in peptide-synthesis-(9-fluorenylmethyloxycarbonyl)-2, 2, 6, 6-tetramethylpiperidine-N-oxyl-4-amino-4-carboxylic acid. J Am Chem Soc 115:11042–11043

Marsh D, Dzikovski BG, Livshits VA (2006) Oxygen profiles in membranes. Biophys J 90:L49–L51

Marsh D, Jost M, Peggion C, Toniolo C (2007) TOAC spin labels in the backbone of alamethicin: EPR studies in lipid membranes. Biophys J 92:473–481

Mchaourab HS, Hyde JS (1993) Dependence of the multiple-quantum EPR signal on the spin–lattice relaxation time. Effect of oxygen in spin-labeled membranes. J Magn Reson B 101:178–184

Mchaourab HS, Perozo E (2000) Determination of protein folds and conformational dynamics using spin labeling EPR spectroscopy. In: Berliner LJ, Eaton SS, Eaton GR (eds) Distance measurements in biological systems by EPR. Kluwer, New York, pp 155–218

Mchaourab HS, Lietzow MA, Hideg K, Hubbell WL (1996) Motion of spin-labeled side chains in T4 lysozyme. Correlation with protein structure and dynamics. Biochemistry 35:7692–7704

Mendel D, Cornish VW, Schultz PG (1995) Site-directed mutagenesis with an expanded genetic code. Annu Rev Biophys Biomol Struct 24:435–462

Merrifield B (1963) Solid phase peptide synthesis. I. The synthesis of a tetrapeptide. J Am Chem Soc 85:2149–2154

Monaco V, Formaggio F, Crisma M, Toniolo C, Hanson P, Millhauser GL et al (1999) Determining the occurence of a 3_{10}-helix and an α-helix in two different segments of a lipopeptaibol antibiotic using TOAC, a nitroxide spin-labeled C^{α}-tetrasubstituted α-aminoacid. Bioorg Med Chem 7:119–131

Nielsen RD, Canaan S, Gladden JA, Gelb MH, Mailer C, Robinson BH (2004) Comparing continuous wave progressive saturation EPR and time domain saturation recovery EPR over the entire motional range of nitroxide spin labels. J Magn Reson 169:129–163

O'Donnell MJ, Bennett WD, Wu S (1989) The stereoselective synthesis of α-amino acids by phase-transfer catalysis. J Am Chem Soc 111:2353–2355

Oganesyan VS (2007) A novel approach to the simulation of nitroxide spin label EPR spectra from a single truncated dynamical trajectory. J Magn Reson 188:196–205

Pannier M, Veit S, Godt A, Jeschke G, Spiess HW (2000) Dead-time free measurement of dipole–dipole interactions between electron spins. J Magn Reson 142:331–340

Perozo E, Cortes DM, Cuello LG (1998) Three-dimensional architecture and gating mechanism of a K^+ channel studied by EPR spectroscopy. Nat Struct Biol 5:459–469

Piton N, Schiemann O, Mu Y, Stock G, Prisner T, Engels JW (2005) Synthesis of spin-labeled RNAS for long range distance measurements by PELDOR. Nucleosides Nucleotides Nucleic Acids 24:771–775

Piton N, Mu Y, Stock G, Prisner TF, Schiemann O, Engels JW (2007) Base-specific spin-labeling of RNA for structure determination. Nucleic Acids Res 35:3128–3143

Plato M, Steinhoff HJ, Wegener C, Törring JT, Savitsky A, Möbius K (2002) Molecular orbital study of polarity and hydrogen bonding effects on the g and hyperfine tensors of site directed NO spin labelled bacteriorhodopsin. Mol Phys 100:3711–3721

Poluektov OG, Utschig LM, Dalosto S, Thurnauer MC (2003) Probing local dynamics of the photosynthetic bacterial reaction center with a cysteine specific spin label. J Phys Chem B 107:6239–6244

Pyka J, Ilnicki J, Altenbach C, Hubbell WL, Froncisz W (2005) Accessibility and dynamics of nitroxide side chains in T4 lysozyme measured by saturation recovery EPR. Biophys J 89:2059–2068

Qin PZ, Hideg K, Feigon J, Hubbell WL (2003) Monitoring RNA base structure and dynamics using site-directed spin labeling. Biochemistry 42:6772–6783

Rabenstein MD, Shin YK (1995) Determination of the distance between 2 spin labels attached to a macromolecule. Proc Natl Acad Sci USA 92:8239–8243

Rassat A, Rey P (1967) Nitroxides, 23: preparation of amino-acid free radicals and their complex salts. Bull Soc Chim Fr 3:815–818

Sale KL, Song L (2005) Explicit treatment of spin labels in modeling of distance constraints from dipolar EPR and DEER. J Am Chem Soc 127:9334–9335

Schiemann O, Prisner TF (2007) Long-range distance determinations in biomacromolecules by EPR spectroscopy. Q Rev Biophys 40:1–53

Schiemann O, Piton N, Plackmeyer J, Bode BE, Prisner TF, Engels JW (2007) Spin labeling of oligonucleotides with the nitroxide TPA and use of PELDOR, a pulse EPR method, to measure intramolecular distances. Nat Protoc 2:904–923

Sezer D, Freed JH, Roux B (2008a) Parametrization, molecular dynamics simulation, and calculation of electron spin resonance spectra of a nitroxide spin label on a polyalanine α-helix. J Phys Chem B 112:5755–5767

Sezer D, Freed JH, Roux B (2008b) Simulating electron spin resonance spectra of nitroxide spin labels from molecular dynamics and stochastic trajectories. J Chem Phys 128: 165106–165116

Shafer AM, Kalai T, Qiao Bin Lui S, Hideg K, Voss JC (2004) Site-specific insertion of spin-labeled L-amino acids in xenopus oocytes. Biochemistry 43:8470–8472

Shin Y-K, Hubbell WL (1992) Determination of electrostatic potentials at biological interfaces using electron–electron double resonance. Biophys J 61:1443–1453

Smirnov AF, Ruuge A, Reznikov VA, Voinov MA, Grigor'ev IA (2004) Site-directed electrostatic measurements with a thiol-specific pH-sensitive nitroxide: differentiating local pK and polarity effects by high-field EPR. J Am Chem Soc 126:8872–8873

Spaltenstein A, Robinson BH, Hopkins PB (1988) A rigid and nonperturbing probe for duplex DNA motion. J Am Chem Soc 110:1299–1301

Spaltenstein A, Robinson BH, Hopkins PB (1989) Sequence- and structure-dependent DNA base dynamics: synthesis, structure, and dynamics of site, and sequence specifically spin-labeled DNA. Biochemistry 28:9484–9495

Steinhoff H-J, Hubbell WL (1996) Calculation of electron paramagnetic resonance spectra from Brownian dynamics trajectories: application to nitroxide side chains in proteins. Biophys J 71:2201–2212

Steinhoff H-J, Dombrowsky O, Karim C, Schneiderhahn C (1991) Two dimensional diffusion of small molecules on protein surfaces: an EPR study of the restricted translational diffusion of protein-bound spin labels. Eur Biophys J 20:293–303

Steinhoff H-J, Mollaaghababa R, Altenbach C, Hideg K, Krebs MP, Khorana HG, Hubbell WL (1994) Time-resolved detection of structural changes during the photocycle of spin-labeled bacteriorhodopsin. Science 266:105–107

Steinhoff H-J, Radzwill N, Thevis W, Lenz V, Brandenburg D, Antson A et al (1997) Determination of interspin distances between spin labels attached to insulin: comparison of electron paramagnetic resonance data with the X-ray structure. Biophys J 73:3287–3298

Steinhoff H-J, Müller M, Beier C, Pfeiffer M (2000a) Molecular dynamics simulation and EPR spectroscopy of nitroxide side chains in bacteriorhodopsin. J Mol Liq 84:17–27

Steinhoff HJ, Savitsky A, Wegener C, Pfeiffer M, Plato M, Möbius K (2000b) High-field EPR studies of the structure and conformational changes of site-directed spin labeled bacteriorhodopsin. Biochim Biophys Acta 1457:253–262

Thorgeirsson TE, Xiao W, Brown LS, Needleman R, Lanyi JK, Shin Y-K (1997) Transient channel-opening in bacteriorhodopsin: an EPR study. J Mol Biol 273:951–957

Vasquez V, Sotomayor M, Marien Cortes D, Roux B, Schulten K, Perozo E (2008) Three-dimensional architecture of membrane-embedded MscS in the closed conformation. J Mol Biol 378: 55–70

Voinov MA, Ruuge A, Reznikov VA, Grigor'ev IA, Smirnov AI (2008) Mapping local protein electrostatics by EPR of pH-sensitive thiol-specific nitroxide. Biochemistry 47:5626–5637

Volkov A, Dockter C, Bund T, Paulsen H, Jeschke G (2009) Pulsed EPR determination of water accessibility to spin-labeled amino acid residues in LHCIIb. Biophys J 96:1124–1141

Ward R, Keeble DJ, El-Mkami H, Norman DG (2007) Distance determination in heterogeneous DNA model systems by pulsed EPR. ChemBioChem 8:1957–1964

Wegener AA, Chizhov I, Engelhard M, Steinhoff H-J (2000) Time-resolved detection of transient movement of helix F in spin-labelled pharaonis sensory rhodopsin II. J Mol Biol 301:881–891

Wegener AA, Klare JP, Engelhard M, Steinhoff H-J (2001) Structural insights into the early steps of receptor–transducer signal transfer in archaeal phototaxis. EMBO J 20:5312–5319

Yin JJ, Pasenkiewicz-Gierula M, Hyde JS (1987) Lateral diffusion of lipids in membranes by pulse saturation recovery electron spin resonance. Proc Natl Acad Sci USA 84:964–968

Zhou Y, Bowler BE, Lynch K, Eaton SS, Eaton GR (2000) Interspin distances in spin-labeled metmyoglobin variants determined by saturation recovery EPR. Biophys J 79:1039–1052